

Optical simulations of a noninvasive technique for the diagnosis of diseased salivary glands *in situ*

I. Gannot^{a)}

Biomedical Engineering Department, Faculty of Engineering, Tel-Aviv University, Tel-Aviv 69978, Israel

R. F. Bonner

Laboratory of Integrative and Medical Biophysics, Section Medical Biophysics, NICHD, NIH, Bethesda, Maryland 20892

G. Gannot and P. C. Fox

Gene Therapy and Therapeutics Branch, NIDR, NIH, Bethesda, Maryland 20892

P. D. Smith

Bioengineering and Physical Sciences Program, ORS, NIH, Bethesda, Maryland 20892

A. H. Gandjbakhche

Laboratory of Integrative and Medical Biophysics, Section on Cell Biophysics, NICHD, NIH, Bethesda, Maryland 20892

(Received 29 January 1997; accepted for publication 31 March 1998)

A simulation experiment for three-dimensional (3D) imaging of exogenous fluoresced antibodies that specifically bind to infiltrating lymphocytes in minor salivary glands was carried out. Small ($\sim 1 \text{ mm}^3$ volume) rhodamine targets, which mimic diseased minor salivary glands labeled with fluorescent antibodies to infiltrating lymphocytes in Sjögren's syndrome, were embedded in a highly scattering tissue phantom consisting of a thick DelrinTM disk covered by index matched DelrinTM slabs of various thickness. In this way the variation of fluorescence profiles on the surface of tissue could be examined corresponding to the range of depths of the salivary glands *in vivo*. Surface images were obtained for different target depths and radial distances from laser excitation to target fluorophore. These images were analyzed and compared to calculations based on random walk theory in turbid media, using previously determined scattering and absorption coefficients of the DelrinTM. Excellent agreement between the surface profiles experimentally measured and those predicted by our random walk theory was obtained. Derivation of these theoretical expressions is a necessary step toward devising an inverse algorithm which may have the potential expressions to perform 3D reconstruction of the concentration distribution of fluorescent labels within tissue. © 1998 American Association of Physicists in Medicine. [S0094-2405(98)01906-3]

Key words: quantitative imaging, exogenous fluorescent markers, random walk, salivary glands, Sjögren syndrome

I. INTRODUCTION

Accurate, simple, and reliable techniques are needed to perform sensitive and specific *in vivo* determinations of abnormalities within a given tissue. When successful, noninvasive "optical biopsies" might replace invasive, destructive biopsies, providing advantages of smaller sampling errors and reduction in cost and time for diagnosis. Moreover, these techniques could integrate simultaneous diagnosis and therapy in "image and treat" procedures, and over time to follow the progression of disease or its regression in response to therapy (e.g., pharmaceutical).

Extensive research has been undertaken on noninvasive optical (visible and infrared) spectroscopic imaging of tissue for tomography, clinical screening, and monitoring of physiological parameters and metabolic status.^{1,2} These techniques can add functional imaging modalities to density imaging, while avoiding ionizing radiation hazards. Differentiation between normal and diseased tissue may be based on differences between the optical properties of normal and diseased

tissue, or those of specific labels targeting pathologies. Several technologically critical elements are required to devise a clinically useful imaging system. These include adequate detected intensity (i.e., signal-to-noise ratio), resolution of the target, and most important, specificity, which is critical for definitive diagnosis.

Tissue surface imaging has been very successful in providing high precision clinical images *in vivo*. However, strong scattering of light by virtually all tissues makes it very difficult to image optically beyond the most superficial layer. Confocal microscopy allows effective rejection of signals arising outside of the selected image plane at depths for which multiple scattering of light by overlying layers is not too great.³ Imaging a number of sequential planes with confocal microscopy enables one to reconstruct three-dimensional (3D) structures within cells and transparent tissues. However, at depths greater than 200 μm in most tissues, out-of-plane diffuse light overwhelms the image from a selected plane, resulting in a loss of contrast and

resolution. This problem in which the ability to achieve necessary intensity at focal spots falls rapidly with increasing depths is also encountered in two-photon excitation.⁴ Moreover, interferometric techniques, such as optical coherence tomography, which have been used for 3D imaging of back-scattered light (though not fluorescence) in the eye or skin, also suffer from multiple scattering which blurs the images coming from deeper than 1 mm in tissue.⁵ The latter can be considered as the average depth at which the direction of the photons is randomized, and after which the photons enter a diffusionlike regime and therefore experience large dispersion in their path lengths. The direct effect of such dispersion is a loss of resolution of an embedded target within the tissue. Although new techniques of time-gated imaging and optical coherence tomography can dramatically increase resolution in turbid tissue by limiting path length dispersion, these techniques are exquisitely sensitive to scattering attenuation ($1/\mu_s \sim 100 \mu\text{m}$). For example, time-resolved transillumination techniques can enhance the resolution by recording those photons which arrive earliest at the detector and hence whose paths deviate least from the optical axis (connecting the source and the detector).^{6,7} However, currently, optical imaging of deep tissue structures leads to resolutions significantly poorer than those attainable with competing techniques based on x rays,⁸ which have proven to be powerful noninvasive diagnostic imaging methods based on weakly specific contrast coupled with high spatial resolution (due to low scatter cross sections). In contrast, the success of any noninvasive, visible or near-IR optical imaging technique must rely on dramatic increases in the specificity of signals arising from abnormal regions embedded in otherwise normal tissue which can compensate for the inherent loss of resolution for deeper structures. Specific intrinsic optical labels have been shown to be used to distinguish between normal and abnormal tissues. For example, autofluorescence associated with metabolic status of cells has been used as markers of disease.⁹⁻¹¹ This approach has led to limited success in tissue surface imaging, e.g., in the detection of Human Papilloma Virus on the surface of the cervix.¹² For deep tissue imaging, complicating factors, such as background fluorescence and multiple scattering, make the quantitation of such fluorescent signals very difficult.

Advances in molecular biology of diseased processes,¹³ new immunohistopathological techniques, and the development of specific fluorescently labeled cell surface markers have led a revolution in specific molecular diagnosis of disease by histopathology as well as in research on molecular origins of disease processes (e.g., using fluorescence microscopy in cell biology). In transparent living preparations, these fluorescent molecular probes have been used *in vitro* for high resolution studies of cell surface dynamics and internal cell activity using confocal or near field microscopy. These advances in specific fluorescent molecular probes suggested to us the possibility of developing specific and quantitative noninvasive diagnosis of tissue changes if appropriate *in vivo* fluorescence imaging techniques can be developed that are clinically practical. Unlike this previous *in vitro* work, quantitation of fluorophore concentration

deeper than 1 mm below the tissue surface requires a theoretical framework which describes photon path dispersion within the tissue.

From the above discussion, clinically practical fluorescence imaging techniques must meet several requirements. First, the pathology under investigation must not lie at a depth where the attenuation of the signal gives poor signal-to-noise ratio and resolvability. Second, the specificity of the marker must be high enough so that one can clearly distinguish between normal and abnormal lesions. Finally, one must have a robust image reconstruction algorithm which enables one to quantify the fluorophore concentration at a given depth.

We have chosen Sjögren's syndrome (SS),¹⁴⁻¹⁷ as an appropriate test case for developing this noninvasive optical biopsy based on 3D localization of exogenous, specific fluorescent labels. SS is an autoimmune disease affecting minor salivary glands which are near (0.5–3.0 mm below) the oral mucosal surface. Therefore the target pathology is relatively accessible to noninvasive optical imaging. The hydraulic conductivity of the oral mucosa is relatively high, which along with the relatively superficial location of the minor salivary glands makes topical application and significant labeling of diseased glands with large fluorescent molecules easier to accomplish. We have shown in *in vitro* labeling studies on tissues containing minor salivary glands that our fluorescent ligands (e.g., fluorescinated antibodies specific to CD+4 T cells¹⁸⁻²⁰ activated lymphocytes infiltrating the salivary glands bind specifically to the infiltrating cells, providing high contrast and a quantitative relationship to their concentration (and therefore to the stage of the disease process). The signal must be higher than background autofluorescence. This background may be further reduced both by spectral isolation from the signal and by using a scanning laser system with deconvolution of multiple images.

We have been developing the random walk theory (RWT)^{21,22} upon which our deconvolution methods will be based and in Sec. II present the results of these calculations. Devising a robust inverse algorithm requires further investigations which are not discussed in the present paper.

II. MATERIAL AND METHODS

This feasibility study simulated *in vivo* tissue optics in a DelrinTM phantom with a corrected scattering coefficient of roughly $\mu'_s = 2 \text{ mm}^{-1}$ as shown in Fig. 1. Embedded rhodamine piece targets of $\sim 1 \mu\text{l}$ volume placed into 1-mm-diam (size of the minor salivary glands) holes simulate localized dense nests of fluorescently labeled lymphocytes infiltrating diseased minor salivary glands. These filled holes were covered with a thin index matching gel (ECHOSINETM—Ultrasound transmission gel) and then DelrinTM slabs (1–6 mm thick) to simulate various depths of fluorescent labels within tissue. The phantom was scanned across its surface with a 30 mW argon laser beam (488 nm) allowing a series of fluorescence images to be obtained for laser excitation at different radial distances from the fluorophore. The digitized two-dimensional (2D) images of the ex-

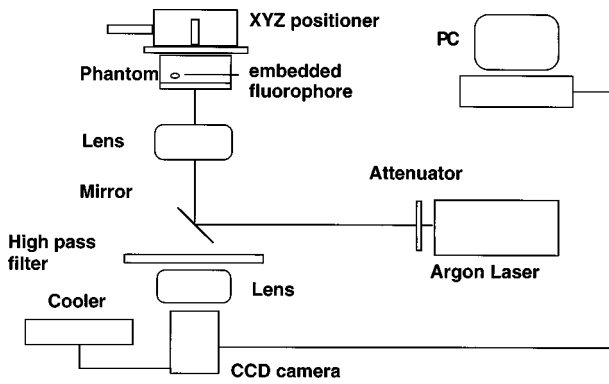


FIG. 1. Experimental setup for the simulation of optical diffusion within the oral mucosa of the lip and excitation of fluorescently labeled antibodies binding to the embedded, diseased minor salivary glands.

cited fluorescence were acquired through a high pass filter with a 3 dB point set between the exciting wavelength and the emission wavelength by a computer controlled charge-coupled device (CCD) camera. Another filter was attached to the CCD surface to attenuate the high brightness of the reflectance of the laser from the surface. Exposure time of the camera was set to cover the whole dynamic range (16 bits) of the camera for each depth. Combinations of distances between excitation location (0–10 mm) and target depths (1–6 mm), varied in 1 mm steps, resulted in 66 different images performed under the same environmental conditions (light, temperature, and humidity). Using the image processing software package NIH Image™ (see <http://rsb.info.nih.gov/ni-image/> for further information and downloading), images were reduced to the 8 most significant bits. An image of a diffuse medium with uniform illumination provided calibration of each pixel in the image system and was used to correct the actual images. This process eliminates the effects of nonlinearities of the imaging system.

An example of surface emission image (converted into a contour plot) of a fluorophore embedded at 1 mm depth and 3 mm distance from the laser source (marked on the image)

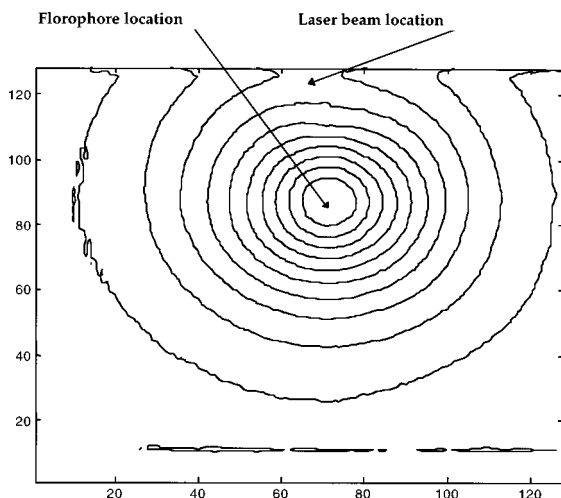


FIG. 2. Surface emission image of standard fluorophore located 1 mm deep and 3 mm from the laser source after correction.

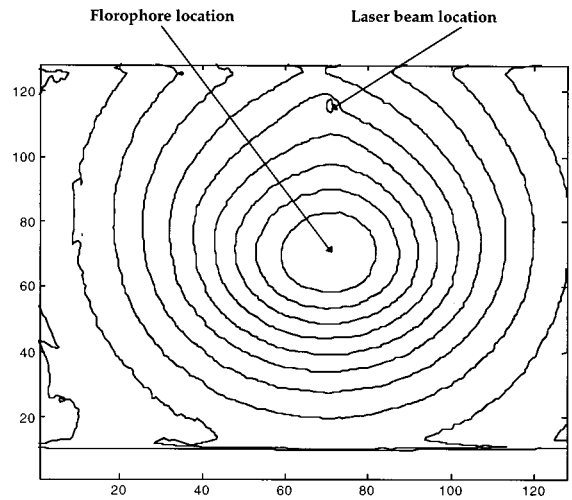


FIG. 3. Surface emission image of standard fluorophore located 3 mm deep and 5 mm from the laser source after correction.

is shown in Fig. 2. In Fig. 3 the image obtained for a fluorophore at 3 mm depth and 5 mm distance from the source is also shown. From these plots, one can immediately see that the image obtained from the deeper fluorophore is shallower than that obtained from the more superficial one. This suggests that the depth information is hidden in the shape of the images as will be shown later. It is not possible to infer the depth and hence the concentration of the fluorophore sites from a single 2D image. In order to predict the actual 3D distribution of the fluorophores, one needs a theoretical development which describes the photon paths inside the tissue and its interactions with the fluorescent site at a given depth. The theoretical analysis used for data analysis is based on the theory of lattice random walk (for detailed derivation see Ref. 24). In this paper, we describe the general description of the model and the final result which will be used subsequently for data analysis.

A schematic drawing describing a photon path is shown in Fig. 4. A typical path can be divided in three processes. First, a photon at the excitation wavelength penetrates into a tissue to a point r_0 before becoming diffusely scattered, then

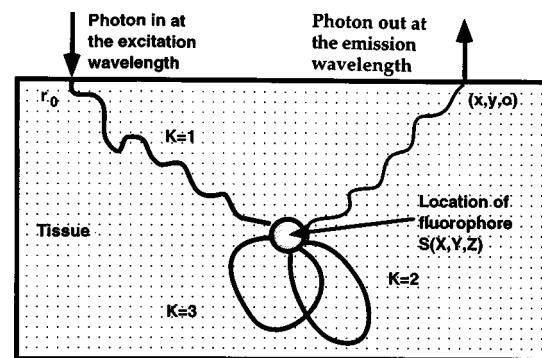


FIG. 4. Schematic drawing of a typical photon path involved in a diffuse fluorescent process. The photon is able to recirculate through the fluorophore site k times before producing an emitted photon, which is detected at the surface.

it travels within the tissue in a diffusionlike process. Then the photon reaching a fluorophore may be absorbed and re-emitted with a longer wavelength with some probability. If the photon is not absorbed by the fluorophore, it is free to migrate further and later return to the fluorescent site a random number of times. The probability of fluorescent emission from an absorbing fluorophore is determined by the quantum efficiency of the fluorophore. Although, in the original derivation, our model included explicitly the finite lifetime of the fluorophore, because our measurement uses cw light, the effect of the lifetime is included in the quantum efficiency. Finally, the fluorescent photon moves from the fluorophore to the tissue surface subjected to the diffusionlike process, though at the emission wavelength.

The parameters which govern this diffuse fluorescent photon migration are: μ_{ai} =absorption coefficient of the excitation wavelength, μ_{ae} =absorption coefficient of the emission wavelength, μ'_{si} =scattering coefficient of the excitation wavelength, μ'_{se} =scattering coefficient of the emission wavelength, $\rho=(x_0, y_0, 0)$ —detection location at the tissue surface, $s=(x_f, y_f, z_f)$ location of the fluorophore (voxel containing the fluorophore), η =probability of exciting the fluorophore ($\sim \mu_{af}$, fluorescence absorption), Φ =quantum efficiency of the fluorophore (here it is close to 1).

The final expression for detected fluorescent intensity at the tissue surface is

$$\hat{G}(\mu_{ai}, \mu_{ae}, \mu'_{si}, \mu'_{se}, x, y_f, z_f, x_0, y_0, \eta) \propto \frac{[H(\alpha_1, \beta_1) - H(\alpha_1, \beta_2) - H(\alpha_2, \beta_1) + H(\alpha_2, \beta_2)]^* \eta}{[1 + \eta(1 + \frac{1}{8}(3/\pi))^{3/2} \sum_{k=1}^{\infty} \exp(-2k(\mu_{ai}/\mu_{ae})) - \eta]} \times \Phi e^{-\mu_{ae}} \tag{1}$$

where

$$H(\alpha, \beta) = \frac{1}{\sqrt{\alpha\beta}} \exp \left[-2 \left(\sqrt{\alpha \left(\frac{\mu_{ai}}{\mu_{si}} \right)} + \sqrt{\beta \left(\frac{\mu_{ae}}{\mu_{se}} \right)} \right) \right] \tag{2}$$

and

$$\alpha_{1,2} = \frac{3}{4} [x_f^2 + y_f^2 + (z_f \pm z_0)^2] (\mu'_{si})^2, \tag{3}$$

$$\beta_{1,2} = \frac{3}{4} [(x - x_0)^2 + (y - y_0)^2 + z_f + z_0 \pm z_0]^2 (\mu'_{se})^2, \tag{4}$$

where

$$z_0 = \sqrt{2} [\mu'_{si,e}]^{-1}. \tag{5}$$

III. RESULTS

In order to compare our theoretical findings with the actual experiments, we measured the optical properties of the Delrin slabs at the incident and emission wavelengths using an integrating spheres method.²³ In this method the total transmission and total reflection of the slabs with known thickness were measured, and using an inverse algorithm based on RWT, the optical parameters μ_a and μ'_s were derived. The results of these calculations yield: $\mu_{ai} = 0.008 \text{ mm}^{-1}$, $\mu_{ae} = 0.004 \text{ mm}^{-1}$, $\mu'_{si} = 1.6 \text{ mm}^{-1}$, $\mu'_{se} = 2.7 \text{ mm}^{-1}$.

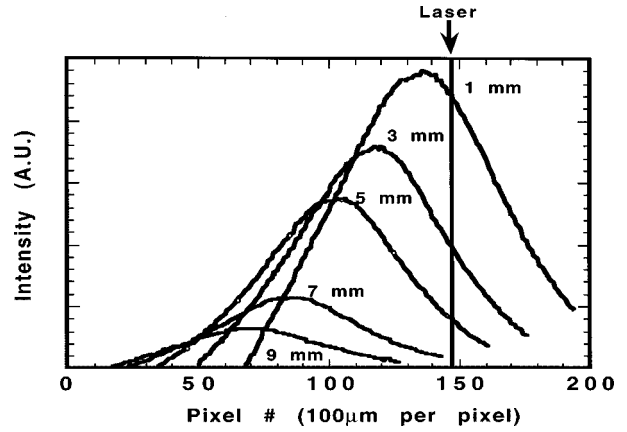


FIG. 5. Fluorescent emission profiles detected at the surface for a 1 mm^3 fluorophore located at a depth of 3 mm in the Delrin™ slab. Radial separation of laser spot and fluorophore is indicated for each curve. The horizontal slices selected contain the laser spot (pixel 148) and fluorescence intensity peak.

Using MATHCAD™, horizontal line scans passing through the maximum of intensity for each image, for five distances between source and fluorophore locations (1, 3, 5, 7, and 9 mm), were analyzed using our RWT. An example of these profile curves, for fluorophores located at 3 mm depth, is shown in Fig. 5. As seen in Fig. 5, the highest peak value is obtained for the nearest fluorophore (1 mm) to the excitation source and lowest one for the remote fluorophore (9 mm). Our theory predicts that for fluorophores located at a given depth, the shape of their center-line scan profiles should be the same.

The emission profiles, shown in Fig. 5, are normalized and shifted to the same location and are shown in Fig. 6. These results show that all normalized emission profiles of fluorophores located at the same depth have similar shape. In Fig. 6, results (the dotted line) of the theoretical calculations of the expression given in Eq. (1), using the optical parameters of the slab at the incident and emission wavelengths

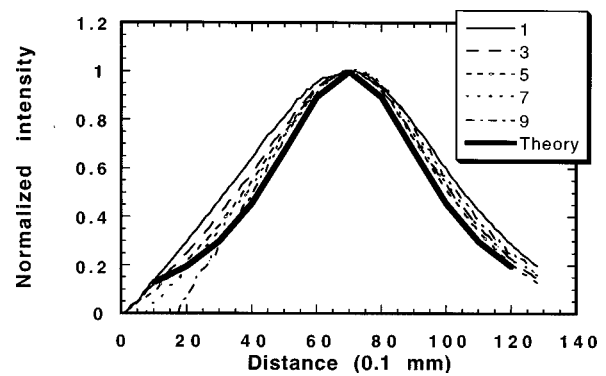


FIG. 6. Comparison of theoretical predictions with measured normalized shapes of fluorescent emission profiles. Surface images were of a fluorophore located at a depth of 3 mm in the Delrin™ slab (as in Fig. 3). According to theory, the radial separation of the laser and fluorophore affects intensity but not the shape of the surface emission profiles. The normalized horizontal slices of the images have been translated to exhibit peak values at pixel 70 for comparison of shapes.

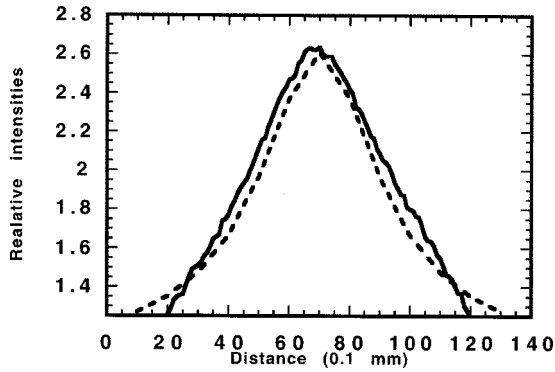


FIG. 7. Ratio of surface intensities for fluorophores embedded 3 and 4 mm deep: --- experiment's results; ---- theory results.

and the depth of the fluorophores site, are also shown. The theory shows a reasonable correlation with experimental results. The same procedure was repeated for other depths of fluorophores and the same good correlation was obtained. We also compared theoretical predictions with experimental results for the ratio of intensities from pairs of fluorophores embedded at different depths. The good correlation between theory and experiment for fluorophores of 3 and 4 mm depth is shown in Fig. 7.

In Fig. 8, we compare the experimental and theoretical falloff of peak fluorescent intensity in the surface image with increasing distance in the *xy* plane between the point of laser irradiation and the fluorophore. The good correlation found from these comparisons between experiments and theoretical predictions (Figs. 6–8), allows us to infer that the shapes of image profiles can be used to determine the depth of embedded fluorophores. The magnitude and position of the intensity peak can then be related to the local concentration of fluorophores at that depth and its 2D location. Ultimately, we hope to devise a complete inverse method utilizing a series of images which allows 3D reconstruction of fluorophore concentration in tissues noninvasively.

To validate these results further, we performed the above described experiments again, but this time used a powder mixture of rhodamine particles and scattering material to simulate more precisely the *in vivo* situation. We have collected the same number of images and performed the same calculations and again received a good agreement between theoretical and experimental results. A representative graph is shown in Fig. 9, where the comparison between two emission profiles of solid rhodamine and the ground rhodamine/Delrin mixture, both at a depth of 5 and 5 mm from excitation location, are presented. In this case the two profiles have fairly similar shapes.

IV. SUMMARY

Our RWT analytical expressions accurately predict intensity distributions in surface fluorescence images obtained as a laser is scanned over the surface of highly scattering phantoms containing focal fluorescent inclusions. Therefore, it appears possible to use these theoretical expressions as the basis for inversion techniques to reconstruct fluorophore

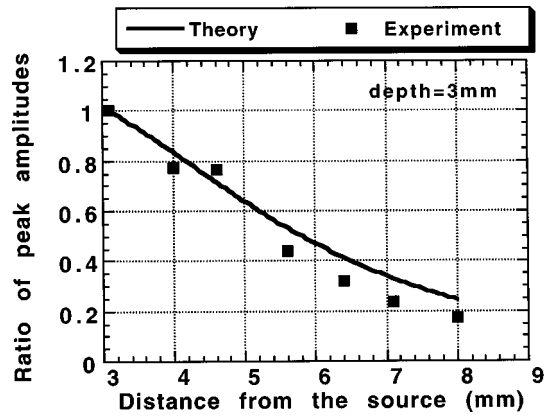


FIG. 8. Comparison between the experimental (squares) and theoretical (solid line) falloff of peak fluorescent intensities in the surface image with increasing distance in the *xy* plane between the point of laser irradiation and the fluorophores. The peak amplitude at 3.1 mm is set to one. The depth of the fluorophores is 3 mm.

source localization and strength. Our next step will be performing experiments with sets of two or more fluorophores with various separations and applying specific inversion techniques based on our RWT expressions to reconstruct fluorophore source localization and strength. *In vivo* optical imaging of the oral mucosa of the lip in SS patients will also be performed along with studies of the binding of fluorescent markers to the infiltrating lymphocytes in the diseased glands and a variety of wash-in and wash-out techniques to maximize specific labeling of the infiltrating lymphocytes while minimizing nonspecific background. We are continuing to refine our system to achieve our main goal of using it clinically to detect and monitor Sjögren's syndrome disease changes and, more generally, to determine applications for exogenous, specific molecular fluorescent labels for quantitative noninvasive *in vivo* diagnosis.

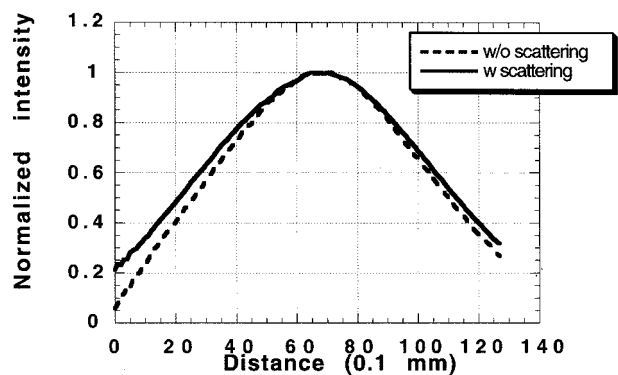


FIG. 9. Comparison of measured normalized shapes of fluorescent emission profiles for a mixture of rhodamine and scattering particles and a full piece of rhodamine. Emission profiles for embedded fluorophore 5 mm deep and 5 mm from exciting laser.

ACKNOWLEDGMENT

The medical part of this work was partially supported by the Sjögren's Syndrome Foundation.

^{a)}Electronic mail: israel@eob.cdrh.fad.gov

¹*Proceedings of Optical Tomography, Photon Migration, and Spectroscopy of Tissue and Model Media: Theory, Human Studies, and Instrumentation*, edited by B. Chance and R. R. Alfano (SPIE, San Jose, CA, 1995), Vol. 2389.

²*Proceedings of Advances in Laser and Light Spectroscopy to Diagnose Cancer And Other Diseases*, edited by R. R. Alfano (SPIE, San Jose, CA, 1995), Vol. 2387.

³J. M. Schmitt, A. Knüttel, and M. Yadlowsky, "Confocal microscopy in turbid media," *J. Opt. Soc. Am. A* **11**, 2226–2235 (1995).

⁴W. Denk, J. H. Strickler, and W. W. Webb, "Two-photon excitation fluorescence scanning microscopy," **248**, 73–75 (1990).

⁵J. M. Schmitt, A. Knüttel, and R. F. Bonner, "Measurement of optical properties of biological tissues by low-coherence interferometry," *Appl. Opt.* **32**, 6032–6042 (1993).

⁶J. C. Hebden, R. A. Kruger, and K. S. Wong, "Time resolved imaging through a highly scattering medium," *Appl. Opt.* **30**, 788–794 (1991).

⁷J. A. Moon and J. Reintjes, "Image resolution by use of multiply scattered light," *Opt. Lett.* **19**, 521–523 (1994).

⁸A. H. Gandjbakhche, R. Nossal, and R. F. Bonner, "Resolution limits for optical transillumination of abnormalities embedded in tissues," *Med. Phys.* **22**, 185–191 (1994).

⁹M. B. Leon, D. Y. Lu, L. G. Prevosti, W. W. Macy, P. D. Smith, M. Granovsky, R. F. Bonner, and R. S. Balaban, "Human arterial surface fluorescence: Atherosclerotic plaque identification and effects of laser atheroma ablation," *J. Am. Coll. Cardiol.* **12**, 94–102 (1988).

¹⁰C. R. Kapadia, F. W. Cutruzzolla, K. M. O'Brien, M. L. Stetz, R. Enriquez, and L. I. Deckelbaum, "Laser-induced fluorescence spectroscopy of human colonic mucosa," *Gastroenterology* **99**, 150–157 (1990).

¹¹R. M. Cothren, R. R. Richards-Kortum, R. P. Rava, G. A. Boyce, M. Doxtader, R. Blackman, T. Ivana, G. B. Hayes, M. S. Feld, and R. E. Petrans, "Gastrointestinal tissue diagnosis by laser-induced fluorescence spectroscopy at endoscopy," *Gastrointest. Endosc.* **36**, 105–111 (1991).

¹²N. Ramanujam, M. F. Mitchell, A. Mahadevan, S. Thomsen, A. Malpica,

T. Wright, N. Atkinson, and R. R. Richards-Kortum, "Development of a multivariate statistical algorithm to analyze human cervical tissue fluorescence spectra acquired *in vivo*," *Lasers Surg. Med.* **19**, 46–62 (1996).

¹³N. S. Nishioka, "Laser Induced Fluorescence Spectroscopy," *Gastrointest. Endosc. Clin. N. Am.* **4**, 313–326 (1994).

¹⁴K. J. Bloch, W. W. Buchanan, M. J. Wohl, and J. J. Bunim, "Sjögren's syndrome," *Medicine* **44**, 187–405 (1965).

¹⁵"Sjögren syndrome," edited by R. I. Fox, *Rheumatic disease clinic of North America* (August 1992).

¹⁶J. S. Greenspan, T. E. Daniels, N. Talal, and R. A. Sylvester, "The histopathology of Sjögren's syndrome in labial salivary gland biopsies," *Oral Surg.* **37**, 217–229 (February 1974).

¹⁷T. E. Daniels, "Labial salivary gland biopsy in Sjögren's syndrome," *Arthritis Rheumatism* **27**, 147–156 (Feb. 1984).

¹⁸T. C. Adamson, R. I. Fox, D. M. Frisman, V. Galanopoulou, J. C. Atkinson, E. S. Jaffe, and H. M. Moutsopoulos, "T cells subpopulations in the labial minor salivary gland histopathologic lesion of Sjögren's syndrome," *J. Rheum.* **18**, 210 (1991).

¹⁹D. Rowe, M. Griffins, J. Stewart, D. Novic, P. C. L. Beverley, and D. A. Isenberg, "HLA class I and II interferon, interleukin-2 and interleukin-2 receptor expression on labial biopsy specimens from patients with Sjögren's syndrome," *Ann. Rheum. Dis.* **46**, 580 (1987).

²⁰J. Coll, S. Thomas, R. Vilella, and J. Corominas, "Interleukin-receptor expression in the salivary glands of patients with Sjögren's syndrome," *J. Rheum.* **22**, 1488 (1995).

²¹A. H. Gandjbakhche and G. H. Weiss, "Random walk and diffusion like models of photon migration in turbid media," *Prog. Opt.* **34**, 332–402 (1995).

²²A. H. Gandjbakhche, R. F. Bonner, I. Gannot, J. Knutson, R. Navai, R. Nossal, and G. H. Weiss, "Fluorescent photon migration theory for turbid biological media," *Adv. Laser Light Spectrosc. Diagnose Cancer Other Diseases III. Opt. Biopsy* **2679**, 8–15 (1996).

²³R. Agah, A.H. Gandjbakhche, M. Motamedi, R. Nossal, and R.F. Bonner, "Dynamics of temperature dependent optical properties of tissues: Dependence on thermal damage," *IEEE Trans. Biomed. Eng.* **43**, 839–846 (1996).

²⁴A. H. Gandjbakhche, R. F. Bonner, R. Nossal, and G. H. Weiss, "Effects of multiple passage probability on fluorescent signals from biological media," *Appl. Opt.* **36**, 4613–4619 (1997).